Al-Kitab Journal for Pure Sciences (2025); 9(2):20-33.
https://doi.org/10.32441/kjps.09.02.p2

Al-Kitab Journal for Pure Sciences
ISSN: 2617-1260 (print), 2617-8141(online)

https://isnra.net/index.php/kjps

An Investigation of the Magnetic and Structural Characteristics of Li-Ni ferrite nanoparticles

Ebtihal G. Khidher

Department of Physics, College of Education for Pure Sciences, University of Kirkuk, Iraq

Corresponding Author: e.gh.abbosh@uokirkuk.edu.iq

Citation: Khidher EG. An Investigation of the Magnetic and Structural Characteristics of Li-Ni ferrite nanoparticles. Al-Kitab J. Pure Sci. [Internet]. 2025 Apr. 13;9(2):20-33. DOI: https://doi.org/10.32441/kjps.09.02.p2.

Keywords: Crystallite Size, Spine1 Ferrites, Sol-Gel Auto-Combustion, Saturation Magnetization.

Received	16 Jan.	2025
Accepted	27 Feb.	2025
Available online	13 Apr.	2025

Abstract:

Nanoparticles of Li-Ni ferrite ($LiNi_{0.5}Fe_2O_4$) were synthesized through the sol-gel auto combustion method, employing lithium nitrate, nickel nitrate, and ferric nitrate as precursors, with citric acid acting as a chelating agent. The samples were annealed at temperatures (as-burnt, from 400 to 800 °C). The impact of various calcination temperatures on the crystalline structure and magnetic characteristics of the $LiNi_{0.5}Fe_2O_4$ nanoparticles was meticulously investigated through X-ray diffraction (XRD) and a vibrating sample magnetometer (VSM).

From XRD analysis, crystallite size D was determined to be the most intense (311) peak using Scherrer's formula. An increase in crystallite size was observed with higher annealing temperatures in the range of 28.50-41.345 nm, while coercivity, with a range 47.9-154.5 Oe, showed an initial rise before decreasing as crystallite size grew. Variations in saturation magnetization (range 6.23-8.02 emu/g) and lattice constant (range 8.291-8.295 °A) displayed a similar trend, decreasing at 400 °C and 600 °C but increasing at 800 °C.

Keywords: Crystallite Size, Spine Ferrites, Sol-Gel; Auto-Combustion, Saturation Magnetization.

دراسة الخصائص المغناطيسية والتركيبية لجسيمات النانوية *Li-Ni* الفراتية

ابتهال غفران خضر

قسم الفيزياء، كلية التربية للعلوم الصرفة، جامعة كركوك، العراق
e.gh.abbosh@uokirkuk.edu.iq

الخلاصة:

تم تحضير الجسيمات النانوية من فيرايت الليثيوم-نيكل ($LiNi_{0.5}Fe_2O_4$) باستخدام تقنية السول-جيل مع الاحتراق الذاتي، حيث استُخدمت نترات الليثيوم، نترات النيكل، ونترات الحديديك كمواد أولية، وتم استخدام حمض الستريك كعامل مخلب. تم تلدين العينات عند درجات حرارة مختلفة (عند الحرق، من ٤٠٠ إلى ٨٠٠ درجة مئوية). تمت دراسة تأثير درجات حرارة التكليس بشكل منهجي على التركيب البلوري والخصائص المغناطيسية لجسيمات $LiNi_{0.5}Fe_2O_4$ النانوية باستخدام حيود الأشعة السينية (*XRD*) ومقياس مغناطيسية العينة الاهتزازي (*VSM*). من تحليل *XRD*، تم تحديد حجم البلورة *D* لأشد قمة (٣١١) باستخدام معادلة شيرر. لوحظت زيادة في حجم البلورات مع ارتفاع درجات حرارة التلدين ضمن نطاق ٢٨,٥٠-٤١,٣٤٥ نانومتر. أظهرت القوة القسرية (٤٧,٩-١٥٤,٥ *Oe*) زيادة أولية ثم انخفاضًا مع زيادة حجم البلورات. كما أظهرت التغيرات في المغناطيسية المشبعة (٦,٢٣-٨,٠٢ *emu/g*) والثابت الشبكي (٨,٢٩١-٨,٢٩٥ *A°*) اتجاهًا مشابهًا، حيث انخفضت عند ٤٠٠°م و٦٠٠°م، لكنها ارتفعت عند ٨٠٠ °م.

الكلمات المفتاحية: حجم البلورات، الفيرايت السبينل، الاحتراق الذاتي؛ السول-جيل، المغناطيسية المشبعة.

1. Introduction:

Ferrite nanoparticles are a significant category of magnetic nanoparticles that have garnered substantial interest due to their extensive uses across many disciplines, from biomedical to industrial [1]. Ferrites have unique magnetic properties, such as the ability to retain magnetism at high temperatures, making them ideal for use in electric motors, transformers, and many other applications [2,3]. Spinel lithium ferrites are characterized by their diverse properties, which can be ascribed to their capacity to accommodate cations of various transition metals inside their lattice structure. Therefore, their structural, optical, magnetic, and electrical properties may vary. Specifically, the compound $Li_{0.5}Fe_{2.5}O_4$ exhibits exceptional features, including high saturation magnetization, low dielectric loss, and a square hysteresis loop, making it a promising magnetic material for use in hybrid nano photocatalysts]4,5[. The rapid progress of wireless communication in the twenty-first century may replace expensive magnetic materials in the fields of antennas and rechargeable lithium-ion batteries.[6] because of its economical price, high Curie temperature, and elevated magnetic permeability.

Ferrite nanoparticles are metal oxides characterised by a spinel structure with the general formula AB_2O_4, wherein A and B represent metallic cations located at distinct crystallographi

csites: tetrahedral (A site) and octahedral (B site)[7]The cations in both places are coordinated to oxygen atoms in tetrahedral and octahedral sites, respectively, as illustrated in **Figure 1**.[8]

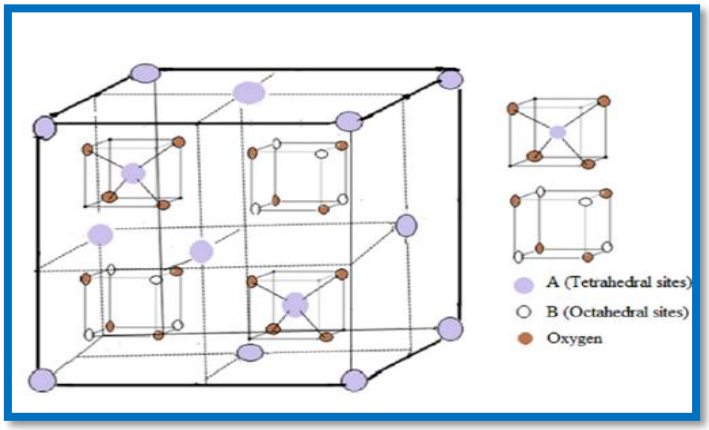

Figure1. Spinel ferrite structure showing tetrahedral and octahedral sites

For a compound to be classified as ferrite, it must contain Fe^{3+} in its chemical formula [9]. Spinel-phase nanocrystalline ferrites $Li_{0.5-0.5x}M_xFe_{2.5-0.5x}O_4$ (where M represents Mg^{2+}, Ni^{2+}, Fe^{2+}, etc) represent one of the most prominent families of nanomaterials due to their wide range of applications, including nano ferrofluids, nanomedical devices, photocatalysts, magnetic devices, microwave devices, and gas sensors [10,11]. The ferrimagnetism of spinel ferrite is attributed to the resultant magnetic moment arising from the antiparallel alignment of magnetic moments at the A and B sites, that is, $\eta_{th} = |\eta_A - \eta_B|$. The replacement of metal cations significantly influences the microstructure and electromagnetic characteristics of lithium ferrite.

Gandomi F. et al. [12], prepared $Li_{0.5}Fe_{2.5}O_4$, $Li\,Mg_{0.5}Fe_2O_4$ and $Li\,Ni_{0.5}Fe_2O_4$ through sol-gel outo-combustion process. The doping of Ni or Mg ions reduces the remanent magnetization (Mr) and saturation magnetization (Ms) of the $LiNi_{0.5}Fe_2O_4$ catalyst. M.F. Warsi et al.[13] prepared praseodymium-substituted nano-crystalline Li-Ni spinel ferrites with different Pr^{3+} contents by micro-emulsion technique. The saturation magnetization (MS) of 41 emu/g and coercivity (HC) of 156.9 Oe for $LiNi_{0.5}Fe_2O_4$ were enhanced through the incorporation of rare earth Pr^{3+} cations.

Innovative methods such as radiofrequency inductively coupled plasma, chemical hydrothermal processes, electrochemical techniques, microwave or non-chemical processing, inert gas condensation, sol-gel auto-combustion, and mechanical milling have been developed for the synthesis of spinel ferrite nanoparticles [14]. The sol–gel auto-combustion process is a prevalent option from this list, utilized in synthesizing materials with various metastable structures, even at very low temperatures, due to its ability to produce products with excellent chemical uniformity. This technology enables the manipulation of physical attributes, including

particle size, shape, and pore structure, by altering the preparation conditions [15]. In addition to the preparation method and metal ion doping, the primary factor affecting the microstructure and performance of ferrite is the sintering temperature.

J. Song et al.[16] investigated the impact of thermal treatment on $Li_{0.35}Nio._3Fe_{2.35}O_4$ using the sol-gel auto-combustion technique. A significant increase in grain size was observed with the rise in annealing temperature. As for coercivity, the value initially increased and subsequently decreased significantly from 115 to 37 Oe with rising annealing temperature. This behavior is attributed to the grain size at 600°C approaching the transitional size between single-domain and multi-domain magnetic regions. R. Paul. Singh et al. [17], prepared magnesium ferrite ($MgFe_2O_4$) nanoparticles using the sol-gel technique, with the samples calcined at different temperatures. The results revealed a significant impact of calcination temperature on the structural and magnetic properties of the nanoparticles. An increase in lattice constant and crystallite size was observed with rising calcination temperature, while coercivity decreased due to the reduction of the pinning effect at the grain boundaries as the calcination temperature increased. According to reports, high sintering temperatures above 1050 °C cause lithium and oxygen to volatilize, changing the stoichiometry of lithium ferrite and so compromising its electrical and magnetic properties [18], significantly reducing the practical use of lithium ferrite.

The structural and magnetic characteristics of $LiNi_{0.5}\ Fe_2O_4$ made using the sol-gel auto-combustion process were investigated in this work. It investigates how temperature changes between 200°C and 800°C affect both its magnetic and crystalline structures.

2. Materials and Methods:

2.1 Material: $LiNi_{0.5}Fe_2O_4$ magnetic nano-powder was prepared using the Sol-Gel Auto-Combustion (SGAC) technique. Lithium nitrate $LiNO_3$, ferric nitrate $Fe\ (NO_3)_3{\cdot}9H_2O$, nickel nitrate $Ni\ (NO_3)_2{\cdot}6H_2O$ citric acid $C_6H_8O_7$ and ammonia with mass 5.745083 g/mol of Lithium nitrate 12.11223 g/mol of Nickel nitrate, 67.3075 g/mol of ferric nitrate and 19.2124 g/mol of citric acid were used as precursors to prepare LiNi0.5Fe2O4 magnetic nano-powders.

2.2 Synthesis $LiNi_{0.5}Fe_2O_4$ magnetic nano-powders: Ferric nitrate, nickel nitrate, and lithium nitrate were dissolved in deionized water at the molar ratios of 2:0.5:1, following the adjustment of the metal nitrate/citric acid ratio at room temperature. Liquid ammonia was added to the mixture to neutralize it to a pH of 7. After that, the neutralized solution was heated to 100°C on a hot plate while being continuously stirred by a magnetic device to evaporate it completely. The solution thickened as the water evaporated, eventually producing an incredibly viscous gel. The gel self-ignited when the temperature was raised to 200°C. The dried gel produced a thick, fluffy powder with a large surface area by continuing a self-sustaining

combustion reaction until it was completely burned. The as-burnt powder was subsequently calcined at various temperatures (400–800°C) for a duration of 3 hours. Experimental observations indicate that all samples exhibited combustible behavior, consistently burning entirely to produce a fine powder.

2.3 Characterization: Phase identification of the calcined powders was performed using a D/MAX-2500 X-ray diffraction (XRD) apparatus with Cu Ka radiation (λ = 1.5405 Å). The samples' magnetic properties were evaluated using a Vibrating Sample Magnetometer (VSM) at room temperature.

3. Results and Discussion

3.1 XRD analysis: The X-ray diffraction for $LiNi_{0.5}Fe_2O_4$ nano particles at various temperatures of calcination (200, 400, 600, and 800 °C) is depicted in **Figure 2**.

The results indicate that with the elevation of calcination temperature, all peaks increase concurrently, leading to narrower and sharper diffraction peaks. This signifies that the increase in particle size within the nucleus leads to a rise in both crystallization density and crystal size ratio.

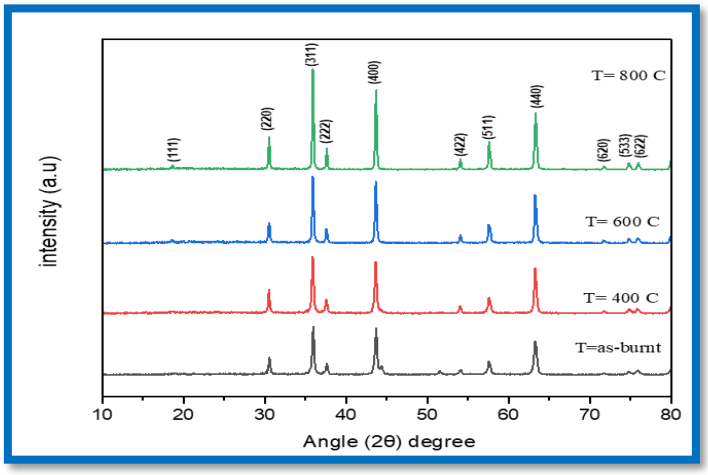

Figure 2. XRD patterns of $LiNi_{0.5}Fe_2O_4$ nanoparticles at various temperatures of calcination

The crystallite size (D) of Li-Ni ferrite, calcined at different temperatures, was determined from the XRD line width of the (311) peak (the greatest intensity peak) using Scherrer's equation **[19]**.

$$D = \frac{k\lambda}{\beta cos\theta} \qquad (1)$$

Where $k = 0.94$ is Scherrer's constant, $\lambda = 1.54$ °A represents the X-ray wavelength, while β denotes the full width at half maximum (FWHM) of the diffraction peak, and θ is the Bragg's angle of diffraction.

Table (1): $LiNi_{0.5}Fe_2O_4$ nanoparticles structural characteristics for as-burnt and different calcination temperatures

Sample	T (°C)	2θ	FWHM	D(nm)	d-spacing (Å)	a (°A)	ρ_x (g/cm3)	LA(°A)	LB (°A)
LiNi0.5Fe2O4	As-burnt	35.98	0.293	28.5003	2.5007	8.294	4.934	3.5914	2.9323
	400	35.91	0.280	29.8249	2.5002	8.292	4.937	3.5907	2.9318
	600	35.94	0.239	34.9443	2.4999	8.291	4.939	3.5902	2.93١3
	800	35.94	0.202	41.3458	2.5011	8.295	4.932	3.5919	2.9328

The calcination temperature significantly influenced the FWHM and crystallite size, as shown in **Table 1** and **Figure 3**. The crystallite size (D) is greatest at 800 °C due to the minimum FWHM value, resulting in enhanced crystallinity of the sample. The value rises from 28.50 nm to 41.34 nm with an increase in an annealing temperature.

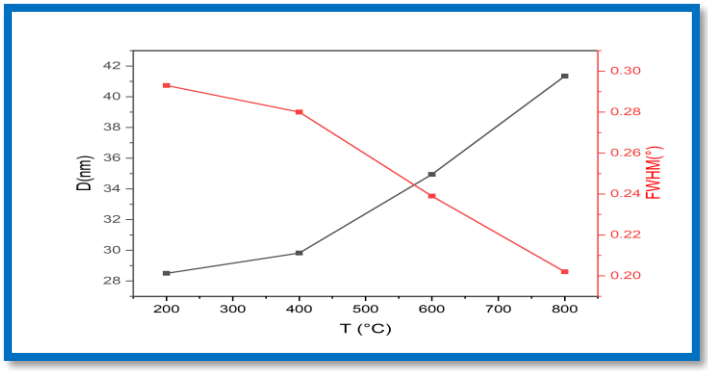

Figure 3. Variation of full width at half maximum (FWHM) and crystallite size as a function of calcination temperature.

The lattice constant (a) exhibits an increase from 8.291 Å to 8.295 Å at calcination temperatures reaching 800 °C, as determined by the following formula **]20[**

$$a = d_{hkl}\sqrt{h^2 + k^2 + l^2} \qquad (2)$$

Where d represents the spacing between the planes, and (h, k, l) denote the Miller indices. A small increase in the lattice constant can be elucidated using Vegard's law, based on the ionic radii of the substituent ions. The substitution of the smaller Fe^{2+} ion (0.64 Å) with the bigger Ni^{2+} ion (0.69 Å) at the octahedral sites is expected to promote an expansion of the unit cell, hence increasing the lattice constant.

X-ray density ρ_x is crucial in evaluating the electromagnetic properties of ferrites, as it is directly linked to the material's crystalline structure and atomic arrangement. These factors significantly influence its electromagnetic characteristics, such as permeability. The equation utilized to find out the X-ray density ρ_x of the samples produced is as **[21]**:

$$\rho_x = \frac{ZM}{Na^3} \qquad (3)$$

Z denotes the number of molecules per unit cell, which is 8 for the spinel structure; M signifies the molecular weight of the corresponding composition; N represents Avogadro's number; and a indicates the lattice constant of the samples. The density (ρ_x) of Li-Ni ferrite ranged between 4.932 and 4.934 g/cm³. The X-ray density was seen to increase with temperature at 400°C and 600°C, then declining at higher temperatures due to its dependence on the lattice parameter a, as shown in **Figure 4**.

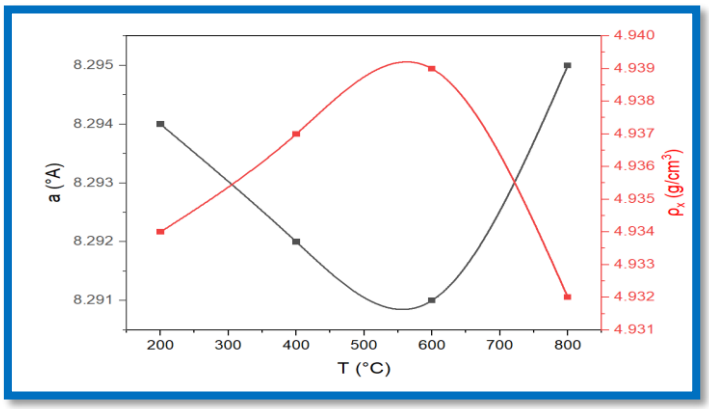

Figure 4. Variation of lattice parameter and X-ray density of the Li-Ni ferrite at various temperatures of calcination

The hopping length is the distance between magnetic ions situated in the tetrahedral (A) and octahedral (B) sites, and it may be calculated using the formulas presented below**[22]**:

$$L_A = 0.25a\sqrt{3} \quad (4)$$

$$L_B = 0.25a\sqrt{2} \quad (5)$$

An alteration in the hopping length on both sides was noticed with an increase in calcination temperature.

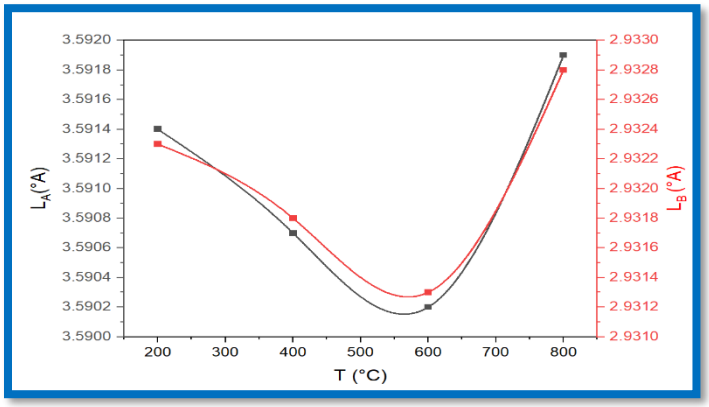

Figure 5. Influence of calcination temperature on the hopping lengths L_A and L_B for Li-Ni ferrite.

As shown in **Figure 5** and **Table 1**, the hopping length L_A is greater than the hopping length L_B , and both vary with temperature changes. This is attributed to the spatial configuration of the tetrahedral sites, which are less constrained compared to the octahedral sites. As the temperature increases, ions such as Fe^{3+} and Ni^{2+} gain kinetic energy, facilitating shifts between

these sites. The lattice parameters are influenced by the reordering of ions, affecting the hopping distances. Furthermore, synthesis conditions, including the annealing process, contribute to the structural arrangement of ions, which in turn impacts the resulting hopping lengths and the associated magnetic properties of the ferrite material.

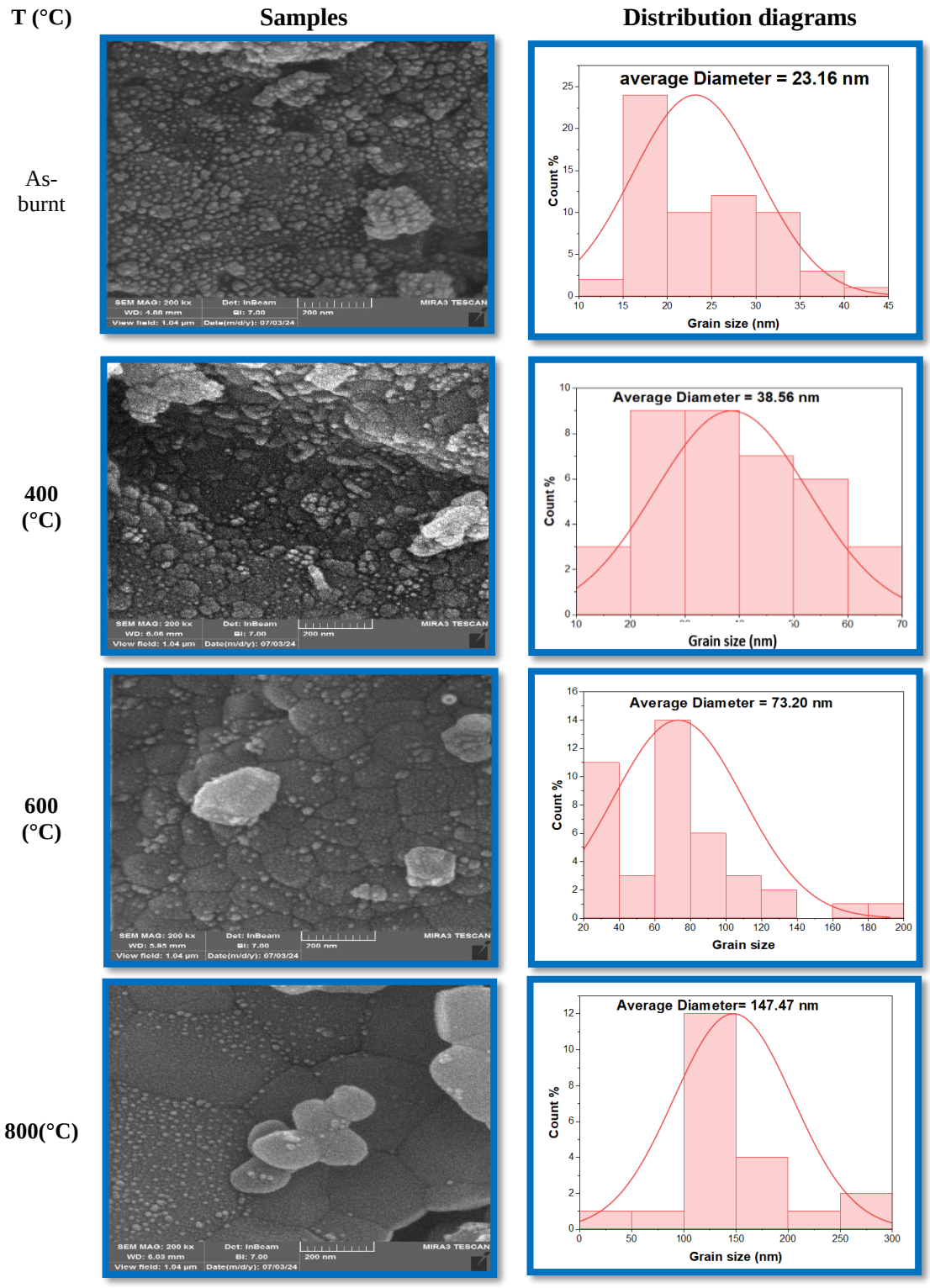

Figure 6. FE-SEM images of $LiNi_{0.5}Fe_2O_4$ nanoparticles at different temperatures.

3.2 FE-SEM: FE-SEM was used to examine the microstructures of the Li-Ni ferrite samples that were synthesized at different calcination temperatures (as-burnt, 400, 600, and 800 °C). The shape of ferrite samples varies from irregular hexagons to spherical aggregates, as seen in **Figure 6**. According to the particle size distribution diagrams shown in **Figure 6** at various calcination temperatures, the samples' grain sizes range from 23.16 nm to 147.47 nm, which is much larger than the values found using Scherrer's formula from XRD analysis, see **Figure 7**. This could be because of lattice strain and molecular structural disorder brought on by the various ionic radii and/or clustering of the nanoparticles. As a result, the XRD approach produces smaller sizes and has stricter criteria. Sintering frequently reduces strain and lattice defects. However, it will result in increased crystallite accumulation, which will lead to an increase in grain size. This is consistent with the pattern of $LiNi_{0.5}Fe_2O_4$ powder grain size at different calcination temperatures.**[23]**

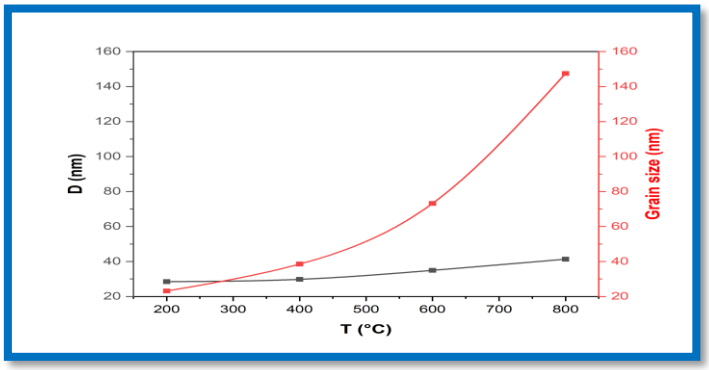

Figure 7. Variation of crystallite size determined by X-ray and grain size of the Li-Ni ferrite at various temperatures of calcination

Table 2: Magnetic properties of $LiNi_{0.5}Fe_2O_4$ nanoparticles for as-burnt and different calcination temperatures.

T(°C)	Ms (emu/g)	Mr (emu/g)	Hc (Oe)	Mr/Ms	*k*(erg/cm3)	$\eta_B(\mu B)$
As-burnt	7.99	2.39	154.3	0.299	1284.2	0.303
400	6.74	2.13	154.5	0.316	1084.7	0.255
600	6.23	1.89	145.9	0.303	946.8	0.236
800	8.02	2.4	47.9	0.299	413.5	0.304

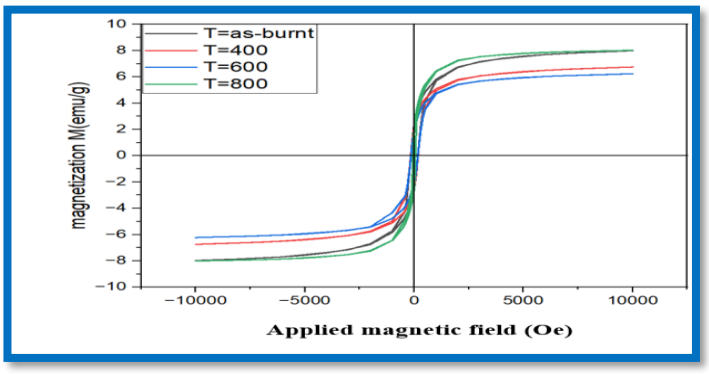

Figure 8. LiNi0.5Fe2O4 nanoparticles hysteresis curves for as-burnt and different calcination temperatures.

3.3 VSM: The M-H loop has been constructed to examine the magnetic characteristics of as-burnt and annealed $LiNi_{0.5}$ Fe_2O_4 nanoparticles. The maximum applied magnetic field was 10 kOe, and measurements were conducted at room temperature. The hysteresis loop provides many magnetic properties, including saturation magnetization (Ms), remanence (Mr), and coercivity (Hc), as shown in **Table 2**.

All samples exhibit soft magnetic characteristics, and the magnetic hysteresis loops get smaller and elongated with rising annealing temperatures, as illustrated in **Figure 8**. The reason is the replacement of the less magnetic Ni^{2+} ions with the magnetic Fe^{3+} ions in the octahedral sublattice of the ferrites, or the occurrence of vacancy crowding in the resulting structure. In general, Extrinsic factors (preparation process, structure, and density) and intrinsic factors (lattice parameter, lattice strain, and cation distribution) significantly affect the material's magnetic behavior.**[24,25]**

The vector sum of a material's magnetic moments per unit mass or volume when the material is magnetized to saturation at a particular temperature while subjected to an external magnetic field is known as saturation magnetization. Neel's model and the cation distribution can be used to explain the samples' magnetism.

This hypothesis posits that exchange interactions are responsible for the magnetic moment in spinel ferrites due to the metal cations located at the A and B sites **[24]**. Magnetic moment (η_B) can be expressed as

$$\eta_B = [M_w \times M_s]/5585 \qquad (6)$$

Where M_w is the molecular weight of the sample, M_s is the saturation magnetization of the sample, and 5585 is the magnetic factor. A decreasing trend is observed in the saturation magnetization and magnetic moment of the nanoparticles at 400 and 600 °C. The decrease in magnetic moment is attributed to the diminished magnetic moments of the A-site (tetrahedral) and B-site (octahedral) lattices, as well as the weakened A-B interactions. The sintering temperature alters the composition of the metal contents. Ni^{2+} and Li^{+} ions predominantly occupy the octahedral sites, with a minority transitioning to the tetrahedral sites as temperature rises **[15]**. The replacement of Fe^{3+} (5μB) with non-magnetic lithium Li^{+} (0μB) leads to a reduction in saturation magnetization at 400 and 600°C; however, at 800°C, the arrangement of Li, Ni, and Fe ions approaches a mixed ferrite state, resulting in an increase of Fe^{3+} (5 μB) in the octahedral position and an elevation of Ni^{2+} (2 μB) in the tetrahedral position, which enhances saturation magnetization. The variations in lattice characteristics and saturation magnetization with respect to annealing temperature are almost the same. **Figure 9** illustrates

the correlation between lattice characteristics and saturation magnetization as a function of calcination temperature.

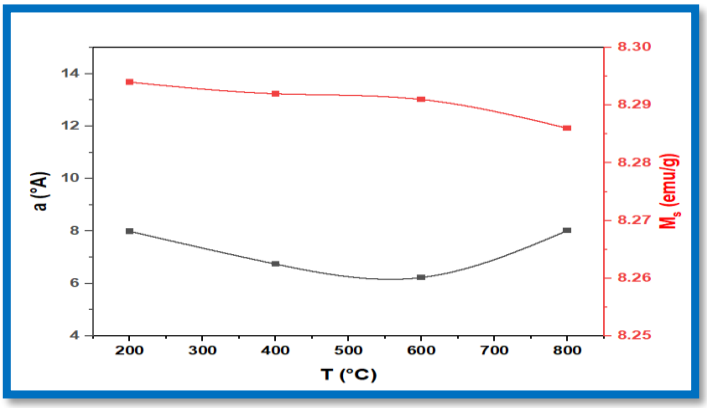

Figure 9. Correlation between lattice parameters (a) and saturation magnetization (Ms) of LiNi0.5Fe2O4 nanoparticles as a function of calcination temperature (T).

Remanent (Mr), usually depends on (M_s), thus by decreasing the saturation magnetization in the prepared samples, remanent magnetization decreases.

Figure 10 illustrates the variation in $LiNi_{0.5}Fe_2O_4$ ferrites' average crystallite size (D) and coercivity (Hc) with respect to calcination temperature (T). The coercivity initially rises and subsequently declines as the crystallite size grows **[26]**. This variation of Hc with crystallite size can be elucidated using the principles of crystal size, single-domain or multi-domain structures, and anisotropy. The anisotropy value was determined using the following equation.:

$$k = \frac{H_c \times M_s}{0.96} \qquad (7)$$

The results are presented in **Table 2**.

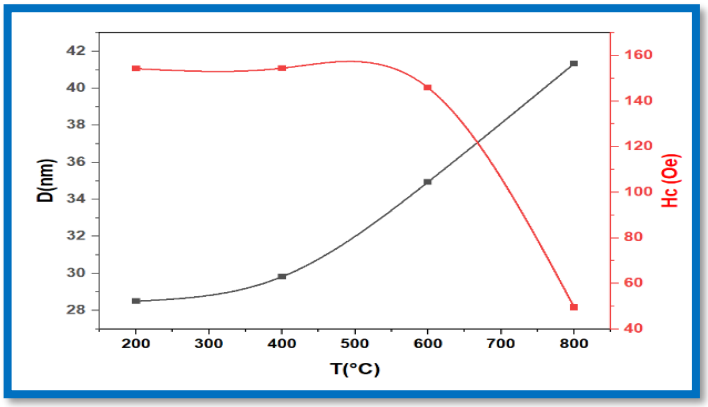

Figure 10. The fluctuation in average crystallite size (D) and coercivity (Hc) of $LiNi_{0.5}Fe_2O_4$ ferrites as a function of calcination temperature (T)

The variation in the anisotropy constant is ascribed to the shape impact of samples manufactured at varying calcination temperatures **[27]**. The hysteresis loops are used to calculate the remanence to saturation magnetization ratio (Mr/Ms) displayed in **Table 2**. The low number also suggests that the ferrites include several domains. According to the results of

this investigation, coercivity peaks at about 400 °C, which is the key temperature at which ferrites change from single-domain to multi-domain behavior.

4. Conclusions

Nano particle Li-Ni ferrites at various calcination temperatures are prepared using the sol-gel auto-combustion technique. The crystallite size D was increased with the calcination temperature up to 800 °C, which was also supported by FE-SEM studies. A maximum saturation magnetization of about 8.02 (emu/g) with a crystallite size of 41.34 nm was obtained at 800 °C, where the variation is almost the same.

5. References

[1] Mullick S. "Ferrites": Synthesis, Structure, Properties and Applications. In 2021. p. 1–61. Available from: https://www.mrforum.com/product/9781644901595-1

[2] Haspers JM. Ferrites: Their properties and applications. In: Modern Materials. Elsevier; 1962. p. 259–341.

[3] Abdulwahab KO, Khan MM, Jennings JR. Ferrites and ferrite-based composites for energy conversion and storage applications. Critical Reviews in Solid State and Materials Sciences [Internet]. 2024 Sep 2;49(5):807–55. Available from: https://www.tandfonline.com/doi/full/10.1080/10408436.2023.2272963

[4] George M, Nair SS, John AM, Joy PA, Anantharaman MR. Structural, magnetic and electrical properties of the sol-gel prepared Li0. 5Fe2. 5O4 fine particles. J Phys D Appl Phys. 2006;39(5):900.

[5] Ahmad M, Shahid M, Alanazi YM, ur Rehman A, Asif M, Dunnill CW. Lithium ferrite (Li0. 5Fe2. 5O4): synthesis, structural, morphological and magnetic evaluation for storage devices. journal of materials research and technology. 2022;18:3386–95.

[6] Zeng H, Tao T, Wu Y, Qi W, Kuang C, Zhou S, et al. Lithium ferrite (Li 0.5 Fe 2.5 O 4) nanoparticles as anodes for lithium ion batteries. RSC Adv. 2014;4(44):23145–8.

[7] Salih SJ, Mahmood WM. Review on magnetic spinel ferrite (MFe2O4) nanoparticles: From synthesis to application. Vol. 9, Heliyon. Elsevier Ltd; 2023.

[8] Issa B, Obaidat IM, Albiss BA, Haik Y. Magnetic nanoparticles: surface effects and properties related to biomedicine applications. Int J Mol Sci. 2013;14(11):21266–305.

[9] Kefeni KK, Msagati TAM, Mamba BB. Ferrite nanoparticles: synthesis, characterisation and applications in electronic device. Materials Science and Engineering: B. 2017;215:37–55.

[10] Gabal MA, El-Shishtawy RM, Al Angari YM. Structural and magnetic properties of nano-crystalline NiZn ferrites synthesized using egg-white precursor. J Magn Magn Mater. 2012;324(14).

[11] Widatallah HM, Johnson C, Gismelseed AM, Al-Omari IA, Stewart SJ, Al-Harthi SH, et al. Structural and magnetic studies of nanocrystalline Mg-doped Li0. 5Fe2. 5O4 particles prepared by mechanical milling. J Phys D Appl Phys. 2008;41(16):165006.

[12] Gandomi F, Peymani-Motlagh SM, Rostami M, Sobhani-Nasab A, Fasihi-Ramandi M, Eghbali-Arani M, et al. Simple synthesis and characterization of Li 0.5 Fe 2.5 O 4, LiMg 0.5 Fe 2 O 4 and LiNi 0.5 Fe 2 O 4, and investigation of their photocatalytic and anticancer properties on hela cells line. Journal of Materials Science: Materials in Electronics. 2019;30:19691–702.

[13] Warsi MF, Gilani ZAA, Al-Khalli NF, Sarfraz M, Khan MAA, Anjum MNN, et al. New LiNi0.5PrxFe2−xO4 nanocrystallites: Synthesis via low cost route for fabrication of smart advanced technological devices. Ceram Int. 2017 Dec 1;43(17):14807–12.

[14] Kaur N, Kaur M. Comparative studies on impact of synthesis methods on structural and magnetic properties of magnesium ferrite nanoparticles, Processing and Application of Ceramics, 8 (2014) 137-143.

[15] Sutka A, Mezinskis G. Sol-gel auto-combustion synthesis of spinel-type ferrite nanomaterials. Front Mater Sci. 2012;6:128–41.

[16] Song J, Wang Z, Gao Y. Effect of heat treatment on structural and magnetic properties of Li–Ni ferrite prepared via sol–gel auto-combustion method. Journal of Materials Science: Materials in Electronics. 2021;32(13):17105–14.

[17] Singh RP, Venkataraju C. Effect of calcinations on the structural and magnetic properties of magnesium ferrite nanoparticles prepared by sol gel method. Chinese journal of physics. 2018;56(5):2218–25.

[18] Surzhikov AP, Malyshev A V, Lysenko EN, Vlasov VA, Sokolovskiy AN. Structural, electromagnetic, and dielectric properties of lithium-zinc ferrite ceramics sintered by pulsed electron beam heating. Ceram Int. 2017;43(13):9778–82.

[19] Ridha SMA. X-ray studies and electrical properties of the zinc-substituted copper nanoferrite synthesized by sol-gel method. Int J Compos Mater. 2015;5(6):195–201.

[20] Mohammad AM, Ridha SMA, Mubarak TH. Dielectric properties of Cr-substituted cobalt ferrite nanoparticles synthesis by citrate-gel auto combustion method. Int J Appl Eng Res. 2018;13(8):6026–35.

[21] Ibrahim MG, Khalf AZ, Ridha SMA. Characterization of Al-Substituted Ni-Zn Ferrites by XRD and FTIR Techniques. Journal of Media,Culture and Communication. 2024 Aug 26;(45):24–39.

[22] Mahmood HN, Razeg KH, Ridha SMA. Study and Analysis of the Structural and Magnetic Properties of Nickel Iron Substituted with Different Proportions of Cerium. Pakistan Journal of Medical & Health Sciences. 2023;17(02):706.

[23] Jumaa JS, Saeed SR, Mohammad AM. Synthesize CoFe2O4/SiO2 nanoparticles and investigate their magnetic, dielectric, and structural characteristics. Passer Journal of Basic and Applied Sciences. 2023;5(2):278–89.

[24] Hassan S, Ahmad M, ur Rehman A, Iqbal MW, Shaukat SF, Abd-Rabboh HSM. Structural, magnetic and electrochemical properties of Al-substituted Ni ferrites for energy storage devices. J Energy Storage. 2022;55:105320.

[25] Kumar Das M, Dey A, Ferdaus J, Chandra Das B, Ahad A, Azizul Hoque M, et al. Investigation of the structural, magnetic, and dielectric properties of Al-substituted Li-Ni-Mn ferrites. Results Phys. 2024 Mar 1;58.

[26] Ramay SM, Saleem M, Atiq S, Siddiqi SA, Naseem S, Sabieh Anwar M. Influence of temperature on structural and magnetic properties of Co 0· 5 Mn 0· 5 Fe 2 O 4 ferrites. Bulletin of Materials Science. 2011;34:1415–9.

[27] Patil RP, Hankare PP, Garadkar KM, Sasikala R. Effect of sintering temperature on structural, magnetic properties of lithium chromium ferrite. J Alloys Compd. 2012;523:66–71.